European Journal of Pharmaceutics and Biopharmaceutics 142 (2019) 531–539

Contents lists available at ScienceDirect

European Journal of Pharmaceutics and Biopharmaceutics

journal homepage: www.elsevier.com/locate/ejpb

Research paper

Spray dried curcumin loaded nanoparticles for antimicrobial photodynamic therapy

Eduard Preis[a], Elias Baghdan[a], Michael R. Agel[a], Thomas Anders[a], Marcel Pourasghar[b], Marc Schneider[b], Udo Bakowsky[a,*]

[a] Department of Pharmaceutics and Biopharmaceutics, University of Marburg, Robert-Koch-Str. 4, 35037 Marburg, Germany
[b] Department of Pharmacy, Biopharmaceutics and Pharmaceutical Technology, Saarland University, Campus C4 1, 66123 Saarbrücken, Germany

ARTICLE INFO

Keywords:
Nanoparticles
Spray drying
Curcumin
Pulmonary drug delivery
Photodynamic therapy
Antimicrobial

ABSTRACT

Antimicrobial resistance is one of the most serious problems that researchers of multiple disciplines are working on. The number of new antibiotics and their targeted structures have continuously decreased emphasizing the demand of alternative therapy for bacterial infections. Photodynamic therapy is such a promising strategy that has been proven to be effective against a wide range of bacterial strains. In this study, an inhalable nano-formulation for photodynamic therapy against respiratory infections was developed in the form of nano-in-microparticles consisting of curcumin nanoparticles embedded in a mannitol matrix. The produced nano-in-microparticles exhibited suitable aerodynamic properties with a mass median aerodynamic diameter of 2.88 ± 0.13 µm and a high fine particle fraction of 60.99 ± 9.50%. They could be readily redispersed in an aqueous medium producing the original nanoparticles without any substantial changes in their properties. This was confirmed using dynamic light scattering and electron microscopy. Furthermore, the redispersed nanoparticles showed an efficient antibacterial photoactivity causing 99.99992% (6.1 $\log_{10}$) and 97.75% (1.6 $\log_{10}$) reduction in the viability of *Staphylococcus saprophyticus* subsp. *bovis* and *Escherichia coli* DH5 alpha respectively. Based on these findings, it can be concluded that nano-in-microparticles represent promising drug delivery systems for antimicrobial photodynamic therapy.

1. Introduction

Lower respiratory tract infections (LRTI) were the leading cause of global years of life lost (YLLs) for both sexes due to premature mortality in 1990. At first, in 2005, they were replaced by ischemic heart disease followed by cerebrovascular disease in 2015, reducing them to third place. However, the total mortality with approximately 2.7 million deaths in 2015 due to LRTI has remained fairly constant from 2005 to 2015 [1]. These numbers summarize the circumstances in different countries all over the world and are mostly results from lack of access to healthcare or effective prevention such as vaccination. Nevertheless, the fact that the respiratory health is continuously exposed to exogenous factors with life-threatening results, e.g. bacteria, fungi, and viruses, represents an undeniable problem [2]. The treatment of LRTI with antibiotics might seem ordinary in most cases, but is often executed incorrectly or unnecessarily [3,4]. Both oral and intravenous routes of administration are common in most guidelines, whereas pulmonary drug delivery of antibiotics is neither recommended nor even mentioned [5–7]. Underlining the importance of this neglected route of administration is the fact that, while some antibiotics penetrate well into the lung tissue [8], others exhibit bad penetration behavior and low concentrations on targeted site [9–14]. Simply increasing the orally

Abbreviations: ACN, acetonitrile; AMR, antimicrobial resistance; aPDT, antimicrobial photodynamic therapy; CFU/mL, colony forming units per milliliter; CLSM, confocal laser scanning microscopy; CUR.NPs, curcumin loaded nanoparticles; DLS, dynamic light scattering; EE, encapsulation efficiency; ELS, electrophoretic light scattering; FDA, U.S. food and drug administration; FPF, fine particle fraction; GSD, geometric standard deviation; LRTI, lower respiratory tract infections; MMAD, mass median aerodynamic diameter; NGI, next generation impactor; NIBS, non-invasive backscatter; NiMps, nano-in-microparticles; NPs, unloaded PLGA nanoparticles; OD_{600}, optical density at $\lambda = 600$ nm; PALS, phase analysis light scattering; PBS, phosphate-buffered saline; PdI, polydispersity index; PLGA, poly(lactic-*co*-glycolic acid); PVA, poly(vinyl alcohol); SEM, scanning electron microscopy; TEM, transmission electron microscopy

* Corresponding author.
E-mail addresses: eduard.preis@pharmazie.uni-marburg.de (E. Preis), elias.baghdan@pharmazie.uni-marburg.de (E. Baghdan), michael.agel@pharmazie.uni-marburg.de (M.R. Agel), thomas.anders@pharmazie.uni-marburg.de (T. Anders), marcel.pourasghar@uni-saarland.de (M. Pourasghar), marc.schneider@mx.uni-saarland.de (M. Schneider), ubakowsky@aol.com (U. Bakowsky).

https://doi.org/10.1016/j.ejpb.2019.07.023
Received 3 June 2019; Received in revised form 24 July 2019; Accepted 26 July 2019
Available online 27 July 2019

or intravenously administered dosage might lead to toxic side effects limiting the applicability of some otherwise more effective drugs [15,16]. These and other facts are the multifactorial foundation of antimicrobial resistance (AMR), one of the most severe problems of mankind [4,17].

Antimicrobial photodynamic therapy (aPDT) utilizes the in situ generation of highly reactive oxygen species targeting multiple cellular structures of the bacteria. It is considered by several research groups that the development of AMR against aPDT is improbable and that multi-antibiotic resistant bacterial strains are as susceptible as naïve strains [18–21]. To overcome limitations due to chemical properties of the photosensitizer, e.g., high hydrophobicity, poor bioavailability, and to enhance its photodynamic activity, different nanoformulations were investigated [22–25]. However, current clinical practice is mostly restricted to intravenous and topical administration showing similar disadvantages as antibiotics in regard to LRTI [26,27].

Over the past decades, different manufacturing processes and formulations for specific inhaler systems gained more and more interest among researchers aiming at high efficacy and applicability in regard of pulmonary drug delivery. Spray drying is one of the most extensively studied processes in the pharmaceutical field. This technique offers many advantages, e.g., high control of particle properties, longer shelf life, and good biocompatibility. Recently, it has been utilized in the preparation of innovative dry powders for inhalation, e.g., nano-in-microparticles (NiMps), also called nano-embedded microparticles or Trojan microparticles [28–31]. Upon contact with the lung fluids, the microparticles should disintegrate and release the embedded nanoparticles providing the beneficial characteristics of these particles.

In this study, curcumin, a naturally occurring photosensitizer with low dark toxicity, was incorporated into poly(lactic-*co*-glycolic acid) (PLGA) nanoparticles [32]. The nanoparticles were embedded in a mannitol matrix (NiMps) by spray drying and an inhalable dry powder was obtained. Morphology, antimicrobial photodynamic activity, and aerodynamic properties were investigated and the benefits in pulmonary drug delivery were evaluated.

2. Materials and methods

2.1. Materials

Poly(lactic-*co*-glycolic acid) (PLGA, Resomer® RG 503H, molecular weight 29,000 g/mol, lactide:glycolide 50:50) was purchased from Evonik Nutrition & Care GmbH (Essen, Germany). Poly(vinyl alcohol) (PVA, Mowiol® 4–88) was a kind gift from Kuraray Europe GmbH (Frankfurt, Germany). Curcumin (≥80%), D-mannitol (≥98%), rhodamine B (for fluorescence), acetonitrile (ACN) were obtained from Sigma-Aldrich Chemie GmbH (Taufkirchen, Germany). Sodium chloride (> 99.8%) was ordered from Carl Roth GmbH (Karlsruhe, Germany), potassium chloride (≥99.5%), di-sodium hydrogen phosphate dihydrate (≥99%) and potassium dihydrogen phosphate (≥99.5%) were all supplied by Merck KGaA (Darmstadt, Germany). Ultrapure water was used for all the experiments. It was generated by PURELAB® flex 4 equipped with a point-of-use biofilter (ELGA LabWater, High Wycombe, UK).

2.2. Bacterial strains and media

Staphylococcus saprophyticus subsp. *bovis* (DSM No. 18669) and *Escherichia coli* DH5 alpha (DSM No. 6897) were obtained from DSMZ (Braunschweig, Germany). Glycerol stock cultures were prepared and stored at −80 °C. One day prior to bacterial viability assay, the stock culture was thawed and cultured overnight in Mueller Hinton broth (MHB, Sigma Aldrich Chemie GmbH) using an orbital shaker (Compact Shaker KS 15 A, equipped with Incubator Hood TH 15, Edmund Bühler GmbH, Bodelshausen, Germany) set at 200 rpm and 37 °C.

2.3. Light source

All irradiation experiments were performed with a custom-made LED device as a light source (Lumundus GmbH, Eisenach, Germany) previously described by Duse et al. [33]. Briefly, multiple arrays of LEDs arranged in parallel were installed in a metal casing covered with a transparent glass and suitable for the irradiation of different multiwell plates. Irradiation time, current, and wavelength were adjustable.

2.4. Preparation of nanoparticles

Curcumin loaded nanoparticles (CUR.NPs) were prepared according to Yallapu et al. with slight modifications [34]. Briefly, 40 mL of 0.5% PVA solution was filled in a 100 mL beaker (aqueous phase) which was placed on a magnetic stirrer (IKA RT 15, IKA®-Werke GmbH & Co. KG., Staufen, Germany) set at 400 rpm. 5 mg curcumin and 200 mg PLGA were dissolved in 10 mL acetone (organic phase), filled in a 10 mL syringe and slowly injected into the aqueous phase. The beaker was left stirring under light protection until the remaining acetone was completely evaporated. Afterwards, the dispersion was transferred into a 50 mL volumetric flask, filled up to the calibration mark with water and divided into 5 mL aliquots which were lyophilized (Christ Alpha 1–4 LSC, Martin Christ Gefriertrocknungsanlagen GmbH, Osterode am Harz, Germany) and stored at 4 °C for further experiments. Unloaded PLGA nanoparticles (NPs) were prepared accordingly without adding curcumin to the organic phase.

2.5. Particle size and ζ-potential

The particle size (hydrodynamic diameter), size distribution, and the ζ-potential were determined by dynamic light scattering (DLS) and electrophoretic light scattering (ELS) respectively using Zetasizer Nano ZS (Malvern Panalytical GmbH, Kassel, Germany). The device was equipped with non-invasive backscatter (NIBS) technology (173°) and phase analysis light scattering (PALS). The samples were diluted 1:100 with phosphate-buffered saline (PBS) (1:100, pH 7.4), filled in a folded capillary cell (DTS1070, Malver Panalytical GmbH) and equilibrated to 25 °C. The attenuation and number of sub-runs were automatically adjusted by the instrument. All measurements were performed in triplicates.

2.6. Encapsulation efficiency (EE)

The nanoparticles were centrifuged at 2,000 *g* for 2 min (Centrifuge 5418, Eppendorf AG, Hamburg, Germany) and the supernatant was carefully removed. A mixture of water and ACN (1:1) was used to dissolve the free curcumin crystals in the formed pellet and the original nanoparticle dispersion was mixed with an equal volume of ACN. The mass of curcumin in the pellet (free) and in the original nanoparticle dispersion (total) was determined by measuring the absorbance with a microplate spectrophotometer (Multiskan® GO, Thermo Scientific, Waltham, MA, USA) at λ = 425 nm. The encapsulation efficiency was calculated according to the following Eq. (1):

$$EE\% = \frac{total\ \ mass\ \ of\ \ curcumin\ \ [mg] - mass\ \ of\ \ free\ \ curcumin\ \ [mg]}{total\ \ mass\ \ of\ \ curcumin\ \ [mg]} \times 100\% \quad (1)$$

2.7. Preparation of nano-in-microparticles (NiMps)

The nanoparticle dispersion was centrifuged at 13,000 *g* and 4 °C for 60 min (Beckman J2-21, Beckman Coulter Inc., CA, USA) and the supernatant was carefully withdrawn. Afterwards, the pellet was redispersed in water with the aid of vortexing and sonication. Mannitol solution (matrix) was added at a mass ratio of 30:70 (PLGA:mannitol) with a final concentration of 1% (m/V). 0.1 wt% rhodamine B based on the mass of mannitol was incorporated for analytical purposes.

Spray drying was performed using the Mini Spray Dryer B-290 (BÜCHI Labortechnik AG, Flawil, Switzerland) equipped with a two-fluid nozzle (inner diameter 0.7 mm). The following process parameters were used: Spray gas flow ~536 L/h, aspirator 100%, inlet temperature 65 °C, outlet temperature < 40 °C, peristaltic pump 7% [31]. The yield was calculated using Eq. (2):

$$yield\,[\%] = \frac{mass\ of\ collected\ spray\ dried\ product\ [mg]}{total\ mass\ of\ solid\ components\ before\ spray\ drying\ [mg]} \times 100\% \quad (2)$$

2.8. Scanning electron microscopy (SEM)

The morphology of nanoparticles and NiMps was investigated with SEM. NPs and CUR.NPs were pipetted on a silica wafer and the water was removed with a low-lint tissue. The samples were washed several times by repeatedly pipetting fresh water on the silica wafer and removing it. NiMps were applied on a silica wafer and loose particles were blown off. All samples were sputter coated with a gold layer of ~15 nm with a current of 20 mA for 50 s (Q150R ES, Quorom Technolgies Ltd, East Grinstead, UK). Images were taken using an acceleration voltage of 5 kV and a secondary electron detector (EVO HD15, Carl Zeiss Microscopy GmbH, Jena, Germany). The particle size distribution and the peak of a gaussian fit were determined by analyzing the SEM micrographs using ImageJ software (version 1.52a, National Institutes of Health, USA) [35].

2.9. Confocal laser scanning microscopy (CLSM)

The colocalization of the embedded nanoparticles within the mannitol matrix was investigated with CLSM. NiMps were placed on a cover slip and loose particles were blown off. Excitation wavelengths of 380 nm and 570 nm were used and detection was performed at 470–556 nm and 566–685 nm for CUR.NPs and rhodamine B labeled mannitol respectively (LSM 710 NLO, Carl Zeiss Microscopy GmbH).

2.10. Redispersibility

The spray dried powder was weighed and redispersed in PBS (pH 7.4) with a final concentration of 15 mg/mL (100 µg/mL curcumin). NiMps disintegration was aided by vortexing for 1 min and sonication for 4 min [36]. The properties of the redispersed nanoparticles were examined by DLS, ELS, and SEM following the aforementioned procedures.

2.11. Aerodynamic properties

The next generation impactor (NGI) (Copley Scientific AG, Therwil, Switzerland) was used to analyze the aerodynamic properties of the spray dried particles. Prior to the experiment approximately 20 mg of the powder was weight and filled into polyethylene capsules (size 3). The inside bottom of all NGI cups was covered with a mixture of 40% of 15% Brij® 35 in ethanol and 60% glycerol. An air flow rate of 60 L/min was adjusted using a flow meter (DFM 2000, Copley Scientific AG), critical flow control (TPK, Copley Scientific AG), and high capacity pump (HCP5, Copley Scientific AG). Inserted into a HandiHaler® (Boehringer Ingelheim, Ingelheim, Germany), the filled capsules were punctured and the content was aerosolized for 4 s. The powder mass retained in the capsule and deposited in the inhaler, induction port, preseparator and all NGI cups was redispersed in water by rinsing and sonication. To determine the respective powder mass, a calibration curve between 0.0025 and 2 mg/mL of the used sample was established and fluorescence measurements were performed at λ_{ex} = 540 nm and λ_{em} = 610 nm using a plate reader (FLUOstar® OPTIMA, Ortenberg, Germany). After plotting the probit values of the cumulative powder mass fractions against the log cut-off diameter, MMAD (mass median aerodynamic diameter), GSD (geometric standard deviation) and FPF (fine particle fraction) were calculated as previously described by Torge et al. [37].

2.12. Antibacterial photoactivity

Both microorganisms (*Staphylococcus saprophyticus* subsp. *bovis* and *Escherichia coli* DH5 alpha) were treated equally, and similar bacterial densities were used. The optical density (OD_{600}) of the overnight culture was measured using a spectrophotometer (Shimadzu UV mini-1240, Kyoto, Japan) and the bacterial suspension was diluted to an OD_{600} of 0.025. The suspension was placed in an orbital shaker (Compact Shaker KS 15 A, equipped with Incubator Hood TH 15, Edmund Bühler GmbH) set at 300 rpm and 37 °C until an OD_{600} of 0.400 was reached. In order to minimize further growth, the bacterial suspension was kept on ice. 200 µL of the bacterial suspension was mixed with 200 µL of CUR.NPs or redispersed NiMps resulting in a total curcumin concentration of 50 µg/mL. Afterwards, the bacterial suspensions were incubated at room temperature for 40 min under light protection. The above-mentioned LED device (Lumundus GmbH) was used as a light source to irradiate the samples in 12-well cell culture plates (TC plate, Standard, F, Nümbrecht, Germany) for 10 min at λ = 457 nm, equivalent to a radiant exposure of 13.2 J/cm^2. After irradiation, a serial dilution of the samples in MHB was plated onto Mueller Hinton II Agar plates (BD, Heidelberg, Germany). After incubating the agar plates for approximately 16 h at 37 °C and 90% relative humidity (In-VitroCell ES NU-5841E, NuAire, Inc., Plymouth, MN, USA), the colonies were counted and the colony forming units per milliliter were calculated (CFU/mL). NPs and PBS (pH 7.4) were used as vehicle control and negative control respectively. Dark controls of all samples were also performed.

2.13. Transmission electron microscopy (TEM)

CUR.NPs and redispersed NiMps were centrifuged at 13,000 *g* and washed twice with PBS (pH 7.4) to minimize the influence of residual PVA and mannitol on imaging respectively. Bacterial cultures were prepared as previously mentioned (2.12) and the growth was stopped at an OD_{600} of 0.400. The bacterial suspensions were centrifuged at 1,000 *g* and washed thrice with PBS (pH 7.4) to remove the residual culture media. Further preparation and staining with 2% uranyl acetate were performed as described by Agel et al. [38]. The particle size distribution and the peak of a gaussian fit was determined as previously described (2.8).

2.14. Statistical analysis

All experiments were performed in triplicates and the results are presented as mean ± standard deviation unless explicitly stated otherwise. To determine significance, two-tailed *t*-test was performed and probability values of $p < 0.05$ were considered significant.

3. Results and discussion

3.1. Physicochemical properties of NPs and CUR.NPs

The nanoparticles were prepared by nanoprecipitation, an established method used to generate nanoparticles with narrow size distribution and high encapsulation efficiency of lipophilic drugs [39,40]. The maximum loading capacity of curcumin in PLGA described by Baghdan et al. was used in this study and all parameters were adjusted in order to achieve optimal particle size and EE [31]. The produced nanoparticles exhibited similar results in terms of size, size distribution (polydispersity index; PdI), and ζ-potential. Hence, curcumin loading did not have any significant influence on the physicochemical properties of NPs and CUR.NPs ($p > 0.05$), which is in agreement with previous studies [31,38]. CUR.NPs showed a monomodal size distribution

Table 1
Particle size (hydrodynamic diameter), polydispersity index (PdI), ζ-potential and encapsulation efficiency (EE). Values are presented as mean ± standard deviation (n = 3).

	Hydrodynamic diameter [nm]	PdI	ζ-potential [mV]	EE [%]
NPs	187.36 ± 12.81	0.07 ± 0.02	−4.12 ± 0.61	–
CUR.NPs	192.58 ± 6.61	0.08 ± 0.03	−4.22 ± 0.35	97.38 ± 0.45
Redispersed NiMps	185.96 ± 16.79	0.11 ± 0.04	−4.71 ± 0.79	–

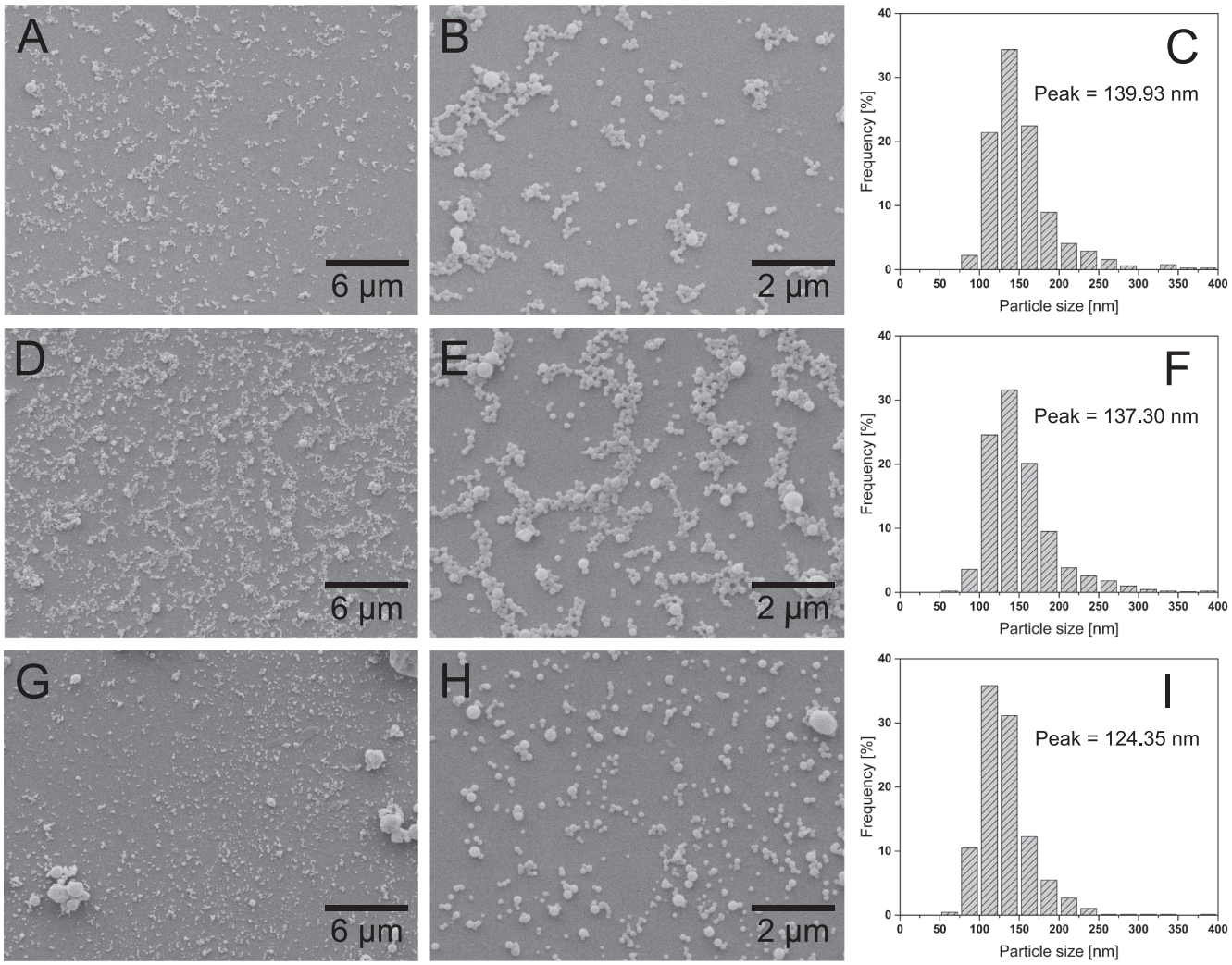

Fig. 1. (A + B): SEM micrographs of unloaded PLGA nanoparticles (NPs), (D + E): SEM micrographs of curcumin loaded PLGA nanoparticles (CUR.NPs), (G + H): SEM micrographs of redispersed CUR.NPs originally embedded in a mannitol matrix (redispersed NiMps), (C + F + I): Particle size analysis of SEM micrographs of NPs, CUR.NPs and redispersed NiMps respectively. Scale bars in A + D + G represent 6 µm. Scale bars in B + E + H represent 2 µm.

(PdI < 0.1) and had a high encapsulation efficiency of approximately 97.38%. The results are summarized in Table 1.

SEM micrographs of the produced nanoparticles confirmed the results obtained by DLS measurements as NPs and CUR.NPs had a comparable particle size of 139.93 nm and 137.30 nm respectively (Fig. 1C and F). However, due to differences in sample preparation and measurement principle, a smaller particle size was observed in the SEM micrographs [41,42]. The particle size obtained by DLS describes the hydrodynamic diameter of the nanoparticles suspended in a certain dispersant, whereas SEM visualizes the particles in its dry form coated with a thin gold layer.

Further investigations of CUR.NPs regarding their particle size and morphology were performed using TEM (Fig. 2). Comparing the results of particle size analysis obtained from SEM (Fig. 1F) and TEM (Fig. 2C), CUR.NPs appeared to have a smaller particle size of 104.27 nm. This can be attributed to the thickness of the gold layer, since sputter coating is unnecessary in TEM.

The morphological characteristics of the produced particles in both SEM and TEM micrographs were comparable, having a spherical shape and a smooth surface.

3.2. Physicochemical properties of the nano-in-microparticles

The preparation of NiMps by spray drying was optimized in respect of high product yield, suitable aerodynamic properties, good redispersibility, and preservation of nanoparticle properties. Therefore, the outlet temperature was carefully kept below the glass transition temperature of PLGA (46.34 °C). Furthermore, comparatively high product yields could be obtained using the high-performance cyclone [43]. After weighing the collected spray dried product, the yield was

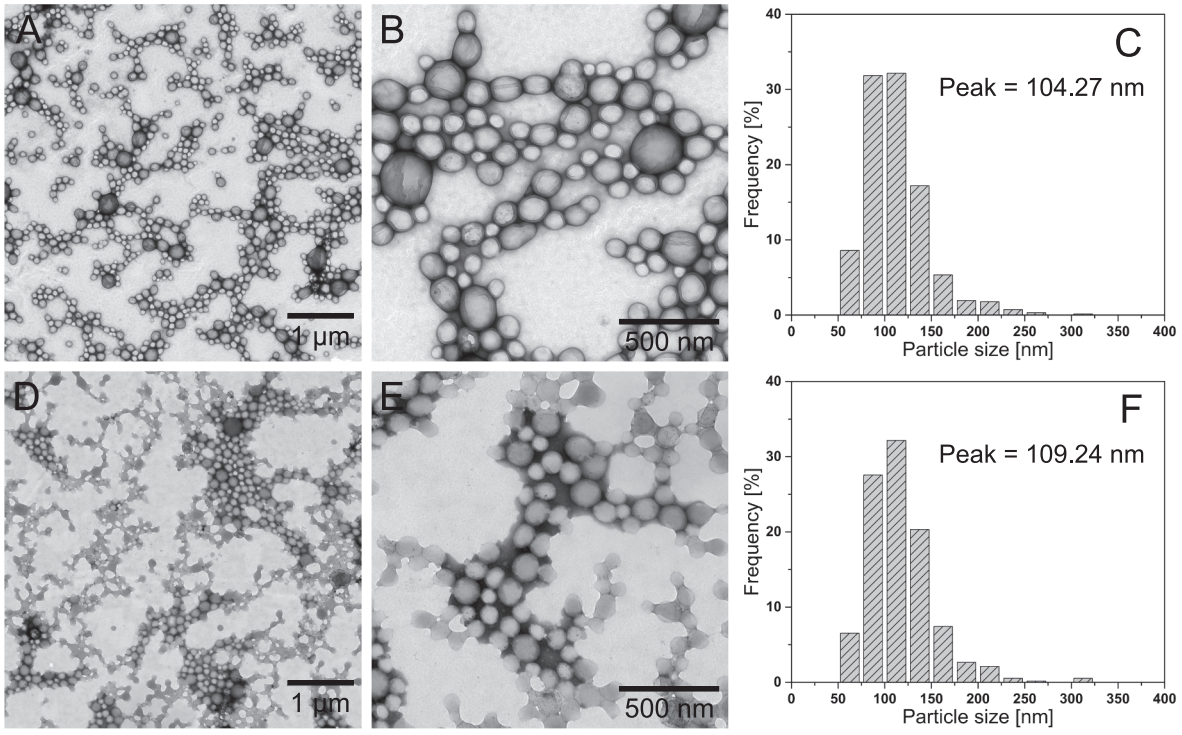

Fig. 2. (A + B): TEM micrographs of curcumin loaded PLGA nanoparticles (CUR.NPs) after negative staining with 2% uranyl acetate, (D + E): TEM micrographs of redispersed CUR.NPs originally embedded in a mannitol matrix (redispersed NiMps) after negative staining with 2% uranyl acetate; (C + F): Particle size analysis of TEM micrographs of CUR.NPs and redispersed NiMps respectively. Scale bars in A + D represent 1 µm. Scale bars in B + E represent 500 nm.

calculated and averaged 61.23 ± 1.67%. Mannitol was chosen as matrix substance due to its benefits in pulmonary drug delivery. It is also an FDA-approved excipient already used in inhaled pharmaceutical products (Exubera®, Pfizer or Aridol®, Pharmaxis) [44]. On the one hand, mannitol increases mucociliary clearance in healthy, asthmatic and bronchiectasis patients based on its osmotic effects. Thereby, the reserve capacity of the mucociliary system can be activated aiding in the removal of pathogens [44–47]. On the other hand, its physicochemical properties, e.g., high water solubility and good aerosolization behavior after spray drying, emphasize its suitability in the field of nano-embedded microparticles [44]. Furthermore, a mass ratio of 30:70 (PLGA:mannitol) was chosen to ensure rapid disintegration and release of nanoparticles at high humidity and at core body temperature (~37 °C), typical conditions present in the lung [37].

SEM micrographs of NiMps (Fig. 3) revealed raisin-shaped hollow particles with wrinkled or dented surfaces. Few smaller microparticles seemed to uphold a rather spherical shape, whereas larger microparticles collapsed due to their hollow structure confirmed by visible holes. In this regard, the Péclet number (*Pe*) has been extensively described in literature to elucidate the low density particle morphology [48]. It relates diffusion time (τ_{diff}) and diffusional motion of the solutes or particles (diffusion coefficient D_i) to the drying time (τ_{dry}), i.e. evaporation rate (κ):

$$Pe = \frac{\tau_{diff}}{\tau_{dry}} = \frac{\kappa}{8D_i} \quad (3)$$

Based on the morphology of NiMps, the drying time seemed to be shorter than the diffusion time resulting in a high Péclet number. As a consequence, the movement of the formed microparticle surface during shrinkage is faster than the diffusion of the suspended nanoparticles. Thus, the surface during the drying process becomes enriched with nanoparticles forming a shell and leading to hollow microparticles [30,37]. SEM micrographs of NiMps revealed a relatively broad particle size distribution ranging from 0.5 to 5 µm.

CLSM images (Fig. 4) were taken to characterize the morphology of NiMps further. They show a homogenous distribution and a colocalization of mannitol (stained with rhodamine B) and CUR.NPs. The center of the particles displays a lower fluorescence underlining the assumption of a hollow structure [37,49].

NiMps could be readily redispersed even at high concentration (15 mg/mL) without negative influences on the particle size and morphology. Different sample preparation methods may have led to

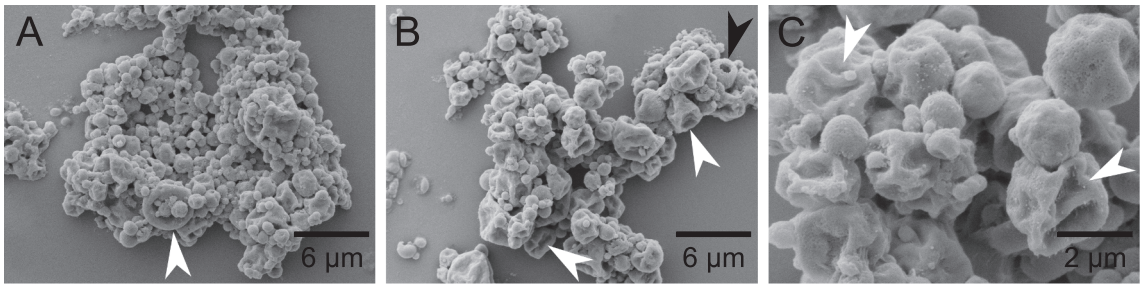

Fig. 3. SEM micrographs of CUR.NPs embedded in a mannitol matrix (NiMps). White arrowheads highlight the collapsed microparticles. Black arrowheads highlight holes in the microparticle surface. Scale bars in A + B represent 6 µm. Scale bar in C represents 2 µm.

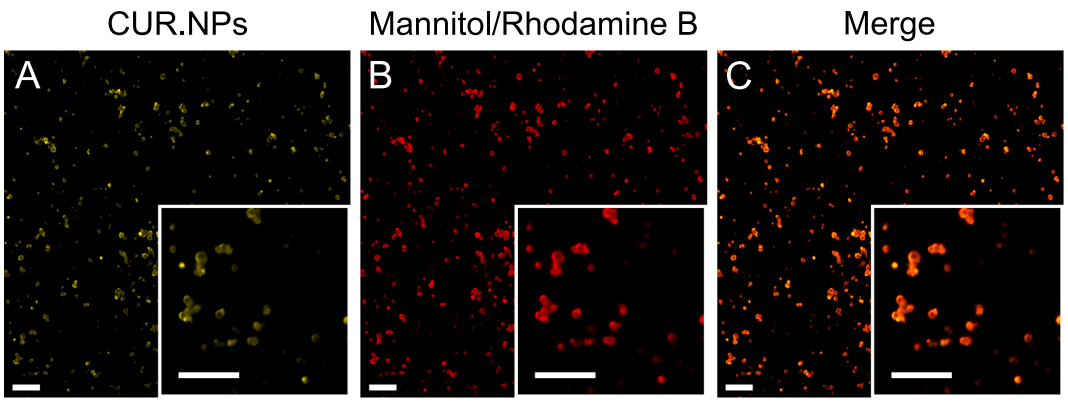

Fig. 4. CLSM images of the nano-in-microparticles showing the homogeneous distribution of CUR.NPs embedded in a mannitol matrix. Scale bars represent 10 µm.

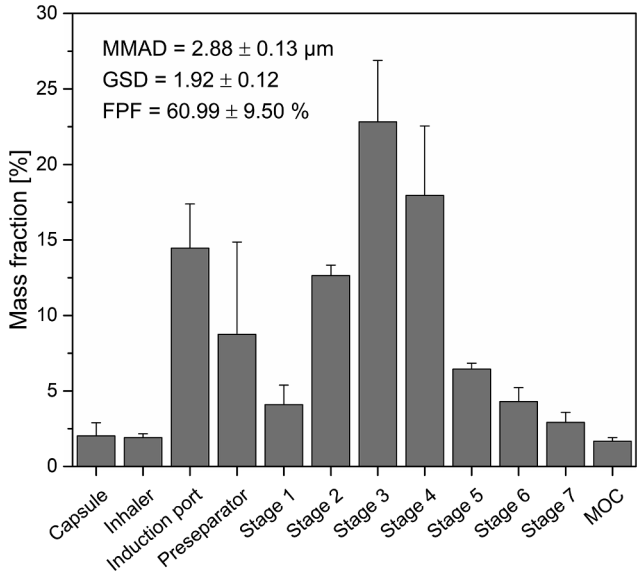

Fig. 5. Mass fraction of the aerosolized powder deposited on different parts of the next generation impactor. Mass median aerodynamic diameter (MMAD), geometric standard deviation (GSD) and fine particle fraction (FPF) were also calculated. Values are presented as mean ± standard deviation.

mannitol residue in SEM and TEM imaging appearing as few larger structures or a diffusive layer on nanoparticles respectively. However, only minor variations in the results of DLS (Table 1), SEM (Fig. 1), and TEM (Fig. 2) comparing NPs and CUR.NPs were observed.

Most pathogens can evade mucociliary clearance and immune response by different mechanisms, one of which is based on their hiding place in thickened mucus plaques [50]. In order to penetrate these plaques, reach their destination, and avoid fast mucociliary clearance, nanoparticles need to possess an optimal particle size since the porous structure of the mucus and the polyvalent low-affinity interactions inhibit the penetration of both larger and smaller particles [51]. Depending on the applied method and mucus types, different pore sizes can be found in literature [52,53]. According to the results of a vertical diffusion chamber system and SEM imaging, Sanders et al. hypothesized pore sizes ranging from approximately 100 nm to 400 nm [52]. Furthermore, Dawson et al. suggested pore sizes between 200 nm and 500 nm utilizing high resolution multiple particle tracking (MPT). Additionally, they presumed that lower negatively charged particles undergo a more rapid transport through mucus than particles with higher charge [54]. Due to the advantages and drawbacks of all these methods, further investigations need to be performed, combining the results of micro- and macroscopical observations [55].

Alveolar macrophages and their internalization of particles represent another clearance mechanism. The internalization of particles is at its maximum in the size range of 0.5 to 5 µm, which is similar to most spray dried particles with ideal aerodynamic properties. In this study, the disintegration of NiMps into their original nanoparticle form would prevent clearance by alveolar macrophages and also be beneficial in regard to mucus penetration [56].

3.3. Aerodynamic properties

Treatment of respiratory infections associated with tuberculosis or chronic disease, e.g., cystic fibrosis, are in need of a selective treatment to avoid long-term systemic antibiosis and adverse effects [56]. In this study, the developed inhalable formulation offers several advantages: photoactive nanoparticles that can utilize the core aspect of aPDT, activation upon irradiation, leading to local effects, and microparticles with appropriate aerodynamic properties for pulmonary drug delivery. The aerodynamic properties have a great influence on the particle deposition inside the lung. By adjusting the aerodynamic diameter, specific parts of the lung can be targeted [56]. The results of the NGI showed a good aerosolization behavior of NiMps with a suitable MMAD of 2.88 µm ± 0.13 µm and a high FPF of 60.99% ± 9.50%. GSD was found to be 1.92 ± 0.12 indicating polydisperse particles. Fig. 5 shows the mass fraction of powder deposited on each part of the NGI after three independent runs. In this case, particle deposition in the lower parts of the lung can be expected which is suitable for the treatment of LRTI and tuberculosis [29].

3.4. Antimicrobial photodynamic activity

The antimicrobial photodynamic activity of CUR.NPs and redispersed NiMps was investigated against both, gram-positive and gram-negative bacterial strains, as there is a proven difference in their susceptibility to antibiotics and photodynamic inactivation. This can be related to the porous layer of peptidoglycan in combination with a single lipid bilayer in gram-positive bacteria, which is easily penetrated by both antibiotics and photosensitizers. On the other hand, the double lipid bilayer of gram-negative bacteria with a smaller peptidoglycan layer in between limits the diffusion and entrance of toxic substances [57].

aPDT using CUR.NPs and redispersed NiMps caused a significant reduction of 99.9991% (5.1 $\log_{10}$) and 99.99992% (6.1 $\log_{10}$) in the viability of *Staphylococcus saprophyticus* subsp. *bovis* respectively. Furthermore, irradiation of CUR.NPs and redispersed NiMps reduced the viability of *Escherichia coli* DH5 alpha significantly by 95.44% (1.3 $\log_{10}$) and 97.75% (1.6 $\log_{10}$) respectively (Fig. 6). In comparison to the negative control, NPs exhibited no effect on the bacterial viability. Additionally, the influence of the light source is negligible since no significant changes in viability could be detected comparing dark and irradiated negative controls. Moreover, CUR.NPs and redispersed

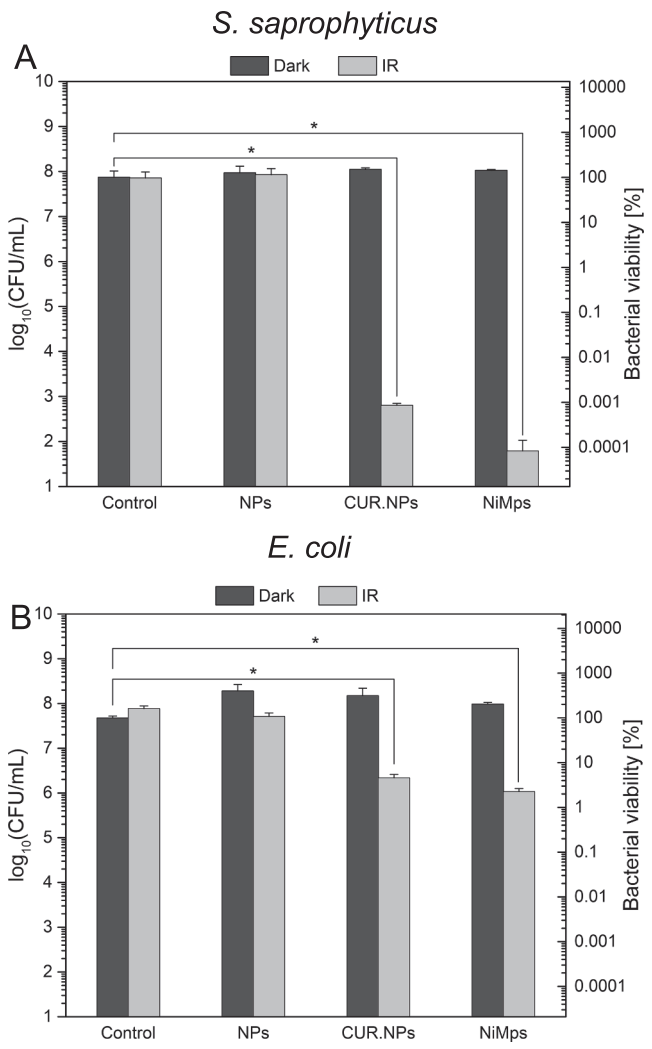

Fig. 6. Bacterial viability of *Staphylococcus saprophyticus* subsp. *bovis* (A) and *Escherichia coli* DH5 alpha (B) upon irradiation (IR) with a custom-made LED device for 10 min at λ = 457 nm (radiant exposure of 13.2 J/cm^2). Unloaded nanoparticles (NPs) and PBS (pH 7.4) were used as vehicle control and negative control respectively. Dark represents unirradiated bacteria. The asterisk denotes probability values of $p < 0.05$ which were considered statically significant.

NiMPs showed no dark toxicity.

The eradication of gram-positive bacteria upon photoactivation of CUR.NPs and redispersed NiMps was higher than that of gram-negative bacteria. Multiple methods to enhance the photodynamic inactivation of gram-negative bacteria were reported, e.g., surface modification of nanoparticles [38], conjugation of photosensitizers and polycationic constructs [58]. They were mostly based on electrostatic interactions, wherein the carrier substance or the photosensitizer itself was modified. In regard to pulmonary drug delivery, a balance between antibacterial efficacy, i.e., high attachment to the bacterial cell wall and mucus penetration, has to be considered. Nanoparticle formulations offer several benefits regarding solubility, stability and selective targeting of photosensitizers. Moreover, the nanoparticles exhibit mechanisms leading to higher permeability by directly interacting with the cell wall and disrupting its three-dimensional organization, thereby increasing the uptake of photosensitizers [22,59]. In aPDT, the position of the photosensitizer in relation to the target structure is crucial since the lifetime of singlet oxygen and its radius of action is short (< 0.02 µm) [60,61]. Due to the low water solubility of curcumin, CUR.NPs and redispersed NiMps need to be in direct proximity to the bacteria.

The structural properties of nanoparticles and their interaction with

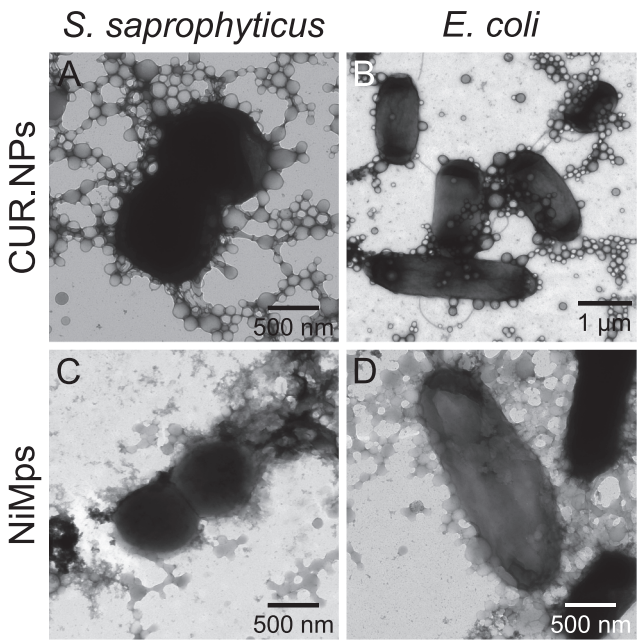

Fig. 7. TEM micrographs after negative staining with 2% uranyl acetate, (A + C): Curcumin loaded PLGA nanoparticles (CUR.NPs) and redispersed CUR.NPs originally embedded in a mannitol matrix (redispersed NiMps) attached to *Staphylococcus saprophyticus* subsp. *bovis* respectively, (B + D): CUR.NPs and redispersed NiMps attached to *Escherichia coli* DH5 alpha respectively. Scale bars in A + C + D represent 500 nm. Scale bar in B represents 1 µm.

bacteria were visualized by TEM. As depicted in Fig. 7, CUR.NPs were directly attached to the surface of *Staphylococcus saprophyticus* subsp. *bovis* and *Escherichia coli* DH5 alpha. Multiple layers of nanoparticles surrounding the bacterial cells were also observed. Mannitol residues were noticed in the TEM images of redispersed NiMps (Fig. 7 C + D). However, mannitol did not alter the antimicrobial photodynamic activity of the redispersed NiMps seen in Fig. 6 or their attachment to the surface of the bacteria. Based on their good redispersibility, attachment on the bacterial cell wall, low dark toxicity, and high photoinactivation, the formulation produced in this study seems ideal for the local therapy of bacterial infections, combining minimal adverse effects and high antibacterial efficacy.

Different types of light source, e.g., diode lasers or dye lasers, have already been used in clinical practice to accomplish photodynamic therapy against lung cancer [62–64]. In combination with small fiber optic delivery systems, that are passed through flexible bronchoscopes, necessary illumination can easily be achieved in the lungs of sedated patients, even penetrating thick lung tissue and reaching peripheral areas [65,66].

4. Conclusions

A curcumin loaded nanoformulation was successfully spray dried and displayed good aerodynamic properties indicating sufficient deposition in the lower respiratory tract. The spray dried nanoparticles exhibited good redispersibility and disintegrated into their original nanoparticle form without experiencing negative changes. The redispersed nanoparticles displayed similar antibacterial activities and attachment to the cell wall compared to the unprocessed samples. The nanoparticles seem to display optimal particle size and low negative surface charge, ideal for mucus penetration and pulmonary drug delivery even after spray drying and redispersion. The penetration of nanoparticles through the mucus is a multifactorial process not only depending on pore size and charge that has to be investigated in further experiments. This groundwork can be modified and used to oppose

severe bacterial infections, reduce antimicrobial resistance and facilitate the treatment of chronic lung disease associated with high risk of infection.

Declaration of Competing Interest

None.

References

[1] H. Wang, M. Naghavi, C. Allen, R.M. Barber, Z.A. Bhutta, A. Carter, D.C. Casey, F.J. Charlson, A.Z. Chen, M.M. Coates, M. Coggeshall, L. Dandona, D.J. Dicker, H.E. Erskine, A.J. Ferrari, C. Fitzmaurice, K. Foreman, M.H. Forouzanfar, M.S. Fraser, N. Fullman, P.W. Gething, E.M. Goldberg, N. Graetz, J.A. Haagsma, S.I. Hay, C. Huynh, C.O. Johnson, N.J. Kassebaum, Y. Kinfu, X.R. Kulikoff, M. Kutz, H.H. Kyu, H.J. Larson, J. Leung, X. Liang, S.S. Lim, M. Lind, R. Lozano, N. Marquez, G.A. Mensah, J. Mikesell, A.H. Mokdad, M.D. Mooney, G. Nguyen, E. Nsoesie, D.M. Pigott, C. Pinho, G.A. Roth, J.A. Salomon, L. Sandar, N. Silpakit, A. Sligar, R.J.D. Sorensen, J. Stanaway, C. Steiner, S. Teeple, B.A. Thomas, C. Troeger, A. VanderZanden, S.E. Vollset, V. Wanga, H.A. Whiteford, T. Wolock, L. Zoeckler, K.H. Abate, C. Abbafati, K.M. Abbas, F. Abd-Allah, S.F. Abera, D.M.X. Abreu, L.J. Abu-Raddad, G.Y. Abyu, T. Achoki, A.L. Adelekan, Z. Ademi, A.K. Adou, J.C. Adsuar, K.A. Afanvi, A. Afshin, E. E. Agardh, A. Agarwal, A. Agrawal, A.A. Kiadaliri, O.N. Ajala, A.S. Akanda, R.O. Akinyemi, T.F. Akinyemiju, N. Akseer, F.H. al Lami, S. Alabed, Z. Al-Aly, K. Alam, N.K.M. Alam, D. Alasfoor, S.F. Aldhahri, R.W. Aldridge, M.A. Alegretti, A.V. Aleman, Z.A. Alemu, L.T. Alexander, S. Alhabib, R. Ali, A.'a. Alkerwi, F. Alla, P. Allebeck, R. Al-Raddadi, U. Alsharif, K.A. Altirkawi, E.A. Martin, N. Alvis-Guzman, A.T. Amare, A.K. Amegah, E.A. Ameh, H. Amini, W. Ammar, S.M. Amrock, H.H. Andersen, B.O. Anderson, G.M. Anderson, C.A.T. Antonio, A.F. Aregay, J. Ärnlöv, V. S.A. Arsenijevic, al Artaman, H. Asayesh, R.J. Asghar, S. Atique, E.F.G.A. Avokpaho, A. Awasthi, P. Azzopardi, U. Bacha, A. Badawi, M.C. Bahit, K. Balakrishnan, A. Banerjee, A. Barac, S.L. Barker-Collo, T. Bärnighausen, L. Barregard, L.H. Barrero, A. Basu, S. Basu, Y.T. Bayou, S. Bazargan-Hejazi, J. Beardsley, N. Bedi, E. Beghi, H. A. Belay, B. Bell, M.L. Bell, A.K. Bello, D.A. Bennett, I.M. Bensenor, A. Berhane, E. Bernabé, B.D. Betsu, A.S. Beyene, N. Bhala, A. Bhalla, S. Biadgilign, B. Bikbov, A.A. B. Abdulhak, B.J. Biroscak, S. Biryukov, E. Bjertness, J.D. Blore, C.D. Blosser, M.A. Bohensky, R. Borschmann, D. Bose, R.R.A. Bourne, M. Brainin, C.E.G. Brayne, A. Brazinova, N.J.K. Breitborde, H. Brenner, J.D. Brewer, A. Brown, J. Brown, T.S. Brugha, G.C. Buckle, Z.A. Butt, B. Calabria, I.R. Campos-Nonato, J.C. Campuzano, J. R. Carapetis, R. Cárdenas, D.O. Carpenter, J.J. Carrero, C.A. Castañeda-Orjuela, J.C. Rivas, F. Catalá-López, F. Cavalleri, K. Cercy, J. Cerda, W. Chen, A. Chew, P.P.-C. Chiang, M. Chibalabala, C.E. Chibueze, O. Chimed-Ochir, V.H. Chisumpa, J.-Y.J. Choi, R. Chowdhury, H. Christensen, D.J. Christopher, L.G. Ciobanu, M. Cirillo, A.J. Cohen, V. Colistro, M. Colomar, S.M. Colquhoun, C. Cooper, L.T. Cooper, M. Cortinovis, B.C. Cowie, J.A. Crump, J. Damsere-Derry, H. Danawi, R. Dandona, F. Daoud, S.C. Darby, P.I. Dargan, J. das Neves, G. Davey, A.C. Davis, D.V. Davitoiu, E. F. de Castro, P. de Jager, D. de Leo, L. Degenhardt, R.P. Dellavalle, K. Deribe, A. Deribew, S.D. Dharmaratne, P.K. Dhillon, C. Diaz-Torné, E.L. Ding, K.P.B. dos Santos, E. Dossou, T.R. Driscoll, L. Duan, M. Dubey, B.B. Duncan, R.G. Ellenbogen, C.L. Ellingsen, I. Elyazar, A.Y. Endries, S.P. Ermakov, B. Eshrati, A. Esteghamati, K. Estep, I.D.A. Faghmous, S. Fahimi, E.J.A. Faraon, T.A. Farid, C.S.e.S. Farinha, A. Faro, M.S. Farvid, F. Farzadfar, V.L. Feigin, S.-M. Fereshtehnejad, J.G. Fernandes, J. C. Fernandes, F. Fischer, J.R.A. Fitchett, A. Flaxman, N. Foigt, F.G.R. Fowkes, E.B. Franca, R.C. Franklin, J. Friedman, J. Frostad, T. Fürst, N.D. Futran, S.L. Gall, K. Gambashidze, A. Gamkrelidze, P. Ganguly, F.G. Gankpé, T. Gebre, T.T. Gebrehiwot, A.T. Gebremedhin, A.A. Gebru, J.M. Geleijnse, B.D. Gessner, A.G. Ghoshal, K.B. Gibney, R.F. Gillum, S. Gilmour, A.Z. Giref, M. Giroud, M.D. Gishu, G. Giussani, E. Glaser, W.W. Godwin, H. Gomez-Dantes, P. Gona, A. Goodridge, S.V. Gopalani, R.A. Gosselin, C.C. Gotay, A. Goto, H.N. Gouda, F. Greaves, H.C. Gugnani, R. Gupta, R. Gupta, V. Gupta, R.A. Gutiérrez, N. Hafezi-Nejad, D. Haile, A.D. Hailu, G.B. Hailu, Y.A. Halasa, R.R. Hamadeh, S. Hamidi, J. Hancock, A.J. Handal, G.J. Hankey, Y. Hao, H.L. Harb, S. Harikrishnan, J.M. Haro, R. Havmoeller, S.R. Heckbert, I.B. Heredia-Pi, P. Heydarpour, H.B.M. Hilderink, H.W. Hoek, R.S. Hogg, M. Horino, N. Horita, H.D. Hosgood, P.J. Hotez, D.G. Hoy, M. Hsairi, A.S. Htet, M.M.T. Htike, G. Hu, C. Huang, H. Huang, L. Huiart, A. Husseini, I. Huybrechts, G. Huynh, K.M. Iburg, K. Innos, M. Inoue, V.J. Iyer, T.A. Jacobs, K.H. Jacobsen, N. Jahanmehr, M.B. Jakovljevic, P. James, M. Javanbakht, S.P. Jayaraman, A.U. Jayatilleke, P. Jeemon, P.N. Jensen, V. Jha, G. Jiang, Y. Jiang, T. Jibat, A. Jimenez-Corona, J.B. Jonas, T.K. Joshi, Z. Kabir, R. Kamal, H. Kan, S. Kant, A. Karch, C.K. Karema, C. Karimkhani, D. Karletsos, G. Karthikeyan, A. Kasaeian, M. Katibeh, A. Kaul, N. Kawakami, J.F. Kayibanda, P.N. Keiyoro, L. Kemmer, A.H. Kemp, A.P. Kengne, A. Keren, M. Kereselidze, C.N. Kesavachandran, Y.S. Khader, I.A. Khalil, A.R. Khan, E.A. Khan, Y.-H. Khang, S. Khera, T.A.M. Khoja, C. Kieling, D. Kim, Y.J. Kim, B.M. Kissela, N. Kissoon, L.D. Knibbs, A.K. Knudsen, Y. Kokubo, D. Kolte, J.A. Kopec, S. Kosen, P.A. Koul, A. Koyanagi, N.H. Krog, B.K. Defo, B.K. Bicer, A.A. Kudom, E.J. Kuipers, V.S. Kulkarni, G.A. Kumar, G.F. Kwan, A. Lal, D.K. Lal, R. Lalloo, T. Lallukka, H. Lam, J. O. Lam, S.M. Langan, C. van Lansingh, A. Larsson, D.O. Laryea, A.A. Latif, A.E.B. Lawrynowicz, J. Leigh, M. Levi, Y. Li, M.P. Lindsay, S.E. Lipshultz, P.Y. Liu, S. Liu, Y. Liu, L.-T. Lo, G. Logroscino, P.A. Lotufo, R.M. Lucas, R. Lunevicius, R.A. Lyons, S. Ma, V.M.P. Machado, M.T. Mackay, J.H. MacLachlan, H.M.A.E. Razek, M. Magdy, A.E. Razek, M. Majdan, A. Majeed, R. Malekzadeh, W.A.A. Manamo, J. Mandisarisa, S. Mangalam, C.C. Mapoma, W. Marcenes, D.J. Margolis, G.R. Martin, J. Martinez-Raga, M.B. Marzan, F. Masiye, A.J. Mason-Jones, J. Massano, R. Matzopoulos, B.M. Mayosi, S.T. McGarvey, J.J. McGrath, M. McKee, B.J. McMahon, P.A. Meaney, A. Mehari, M.M. Mehndiratta, F. Mejia-Rodriguez, A.B. Mekonnen, Y.A. Melaku, P. Memiah, Z.A. Memish, W. Mendoza, A. Meretoja, T.J. Meretoja, F.A. Mhimbira, R. Micha, A. Millear, T.R. Miller, M. Mirarefin, A. Misganaw, C.N. Mock, K.A. Mohammad, A. Mohammadi, S. Mohammed, V. Mohan, G.L.D. Mola, L. Monasta, J. C.M. Hernandez, P. Montero, M. Montico, T.J. Montine, M. Moradi-Lakeh, L. Morawska, K. Morgan, R. Mori, D. Mozaffarian, U.O. Mueller, G.V.S. Murthy, S. Murthy, K.I. Musa, J.B. Nachega, G. Nagel, K.S. Naidoo, N. Naik, L. Naldi, V. Nangia, D. Nash, C. Nejjari, S. Neupane, C.R. Newton, J.N. Newton, M. Ng, F.N. Ngalesoni, J. de Dieu Ngirabega, Q. Le Nguyen, M.I. Nisar, P.M.N. Pete, M. Nomura, O.F. Norheim, P.E. Norman, B. Norrving, L. Nyakarahuka, F.A. Ogbo, T. Ohkubo, F. A. Ojelabi, P.R. Olivares, B.O. Olusanya, J.O. Olusanya, J.N. Opio, E. Oren, A. Ortiz, M. Osman, E. Ota, R. Ozdemir, M. PA, A. Pain, J.D. Pandian, P.R. Pant, C. Papachristou, E.-K. Park, J.-H. Park, C.D. Parry, M. Parsaeian, A.J.P. Caicedo, S.B. Patten, G.C. Patton, V.K. Paul, N. Pearce, J.M. Pedro, L.P. Stokic, D.M. Pereira, N. Perico, K. Pesudovs, M. Petzold, M.R. Phillips, F.B. Piel, J.D. Pillay, D. Plass, J.A. Platts-Mills, S. Polinder, C.A. Pope, S. Popova, R.G. Poulton, F. Pourmalek, D. Prabhakaran, M. Qorbani, J. Quame-Amaglo, D.A. Quistberg, A. Rafay, K. Rahimi, V. Rahimi-Movaghar, M. Rahman, M.H.U. Rahman, S.U. Rahman, R.K. Rai, Z. Rajavi, S. Rajsic, M. Raju, I. Rakovac, S.M. Rana, C.L. Ranabhat, T. Rangaswamy, P. Rao, S.R. Rao, A.H. Refaat, J. Rehm, M.B. Reitsma, G. Remuzzi, S. Resnikoff, A.L. Ribeiro, S. Ricci, M.J.R. Blancas, B. Roberts, A. Roca, D. Rojas-Rueda, L. Ronfani, G. Roshandel, D. Rothenbacher, A. Roy, N.K. Roy, G.M. Ruhago, R. Sagar, S. Saha, R. Sahathevan, M.M. Saleh, J.R. Sanabria, M.D. Sanchez-Niño, L. Sanchez-Riera, I.S. Santos, R. Sarmiento-Suarez, B. Sartorius, M. Satpathy, M. Savic, M. Sawhney, M.P. Schaub, M.I. Schmidt, I.J.C. Schneider, B. Schöttker, A.E. Schutte, D.C. Schwebel, S. Seedat, S.G. Sepanlou, E.E. Servan-Mori, K.A. Shackelford, G. Shaddick, A. Shaheen, S. Shahraz, M.A. Shaikh, M. Shakh-Nazarova, R. Sharma, J. She, S. Sheikhbahaei, J. Shen, Z. Shen, D.S. Shepard, K.N. Sheth, B.P. Shetty, P. Shi, K. Shibuya, M.-J. Shin, R. Shiri, I. Shiue, M.G. Shrime, I.D. Sigfusdottir, D.H. Silberberg, D.A.S. Silva, D.G. A. Silveira, J.I. Silverberg, E.P. Simard, A. Singh, G.M. Singh, J.A. Singh, O.P. Singh, P.K. Singh, V. Singh, S. Soneji, K. Søreide, J.B. Soriano, L.A. Sposato, C.T. Sreeramareddy, V. Stathopoulou, D.J. Stein, M.B. Stein, S. Stranges, K. Stroumpoulis, B.F. Sunguya, P. Sur, S. Swaminathan, B.L. Sykes, C.E.I. Szoeke, R. Tabarés-Seisdedos, K.M. Tabb, K. Takahashi, J.S. Takala, R.T. Talongwa, N. Tandon, M. Tavakkoli, B. Taye, H.R. Taylor, B.J.T. Ao, B.A. Tedla, W.M. Tefera, M. ten Have, A.S. Terkawi, F.H. Tesfay, G.A. Tessema, A.J. Thomson, A.L. Thorne-Lyman, A.G. Thrift, G.D. Thurston, T. Tillmann, D.L. Tirschwell, M. Tonelli, R. Topor-Madry, F. Topouzis, J.A. Towbin, J. Traebert, B.X. Tran, T. Truelsen, U. Trujillo, A.K. Tura, E.M. Tuzcu, U.S. Uchendu, K.N. Ukwaja, E.A. Undurraga, O.A. Uthman, R. van Dingenen, A. van Donkelaar, T. Vasankari, A.M.N. Vasconcelos, N. Venketasubramanian, R. Vidavalur, L. Vijayakumar, S. Villalpando, F.S. Violante, V. V. Vlassov, J.A. Wagner, G.R. Wagner, M.T. Wallin, L. Wang, D.A. Watkins, S. Weichenthal, E. Weiderpass, R.G. Weintraub, A. Werdecker, R. Westerman, R.A. White, T. Wijeratne, J.D. Wilkinson, H.C. Williams, C.S. Wiysonge, S.M. Woldeyohannes, C.D.A. Wolfe, S. Won, J.Q. Wong, A.D. Woolf, D. Xavier, Q. Xiao, G. Xu, B. Yakob, A.Z. Yalew, L.L. Yan, Y. Yano, M. Yaseri, P. Ye, H.G. Yebyo, P. Yip, B.D. Yirsaw, N. Yonemoto, G. Yonga, M.Z. Younis, S. Yu, Z. Zaidi, M.E.S. Zaki, F. Zannad, D.E. Zavala, H. Zeeb, B.M. Zeleke, H. Zhang, S. Zodpey, D. Zonies, L.J. Zuhlke, T. Vos, A.D. Lopez, C.J.L. Murray, Global, regional, and national life expectancy, all-cause mortality, and cause-specific mortality for 249 causes of death, 1980–2015: a systematic analysis for the Global Burden of Disease Study 2015, Lancet 388 (2016) 1459–1544.

[2] Forum of International Respiratory Societies, The global impact of respiratory disease, Second edition ed., European Respiratory Society, Sheffield, 2017.

[3] D.J. Shapiro, L.A. Hicks, A.T. Pavia, A.L. Hersh, Antibiotic prescribing for adults in ambulatory care in the USA, 2007–09, J. Antimicrob. Chemother. 69 (2014) 234–240.

[4] J. O'Neill, Tackling drug-resistant infections globally: Final report and recommendations. The review on antimicrobial resistance, 2016.

[5] K. Dalhoff, M. Abele-Horn, S. Andreas, M. Deja, S. Ewig, P. Gastmeier, S. Gatermann, H. Gerlach, B. Grabein, C.P. Heußel, G. Höffken, M. Kolditz, E. Kramme, H. Kühl, C. Lange, K. Mayer, I. Nachtigall, M. Panning, M. Pletz, P.-M. Rath, G. Rohde, S. Rosseau, B. Schaaf, D. Schreiter, H. Schütte, H. Seifert, C. Spies, T. Welte, Epidemiologie, diagnostik und therapie erwachsener patienten mit nosokomialer pneumonie – update 2017, Pneumologie (Stuttgart, Germany) 72 (2018) 15–63.

[6] S. Ewig, G. Höffken, W.V. Kern, G. Rohde, H. Flick, R. Krause, S. Ott, T. Bauer, K. Dalhoff, S. Gatermann, M. Kolditz, S. Krüger, J. Lorenz, M. Pletz, A. de Roux, B. Schaaf, T. Schaberg, H. Schütte, T. Welte, Behandlung von erwachsenen Patienten mit ambulant erworbener pneumonie und prävention - update 2016, Pneumologie (Stuttgart, Germany) 70 (2016) 151–200.

[7] M. Woodhead, F. Blasi, S. Ewig, J. Garau, G. Huchon, M. Ieven, A. Ortqvist, T. Schaberg, A. Torres, G. van der Heijden, R. Read, T.J.M. Verheij, Guidelines for the management of adult lower respiratory tract infections–full version, Clin. Microbiol. Infect. Offic. Public. Euro. Soc. Clin. Microbiol. Infect. Dis. 17 (Suppl 6) (2011) E1–E59.

[8] R. Wise, D. Honeybourne, Pharmacokinetics and pharmacodynamics of fluoroquinolones in the respiratory tract, Euro. Respirat. J. 14 (1999) 221–229.

[9] M. Bassetti, C.-E. Luyt, D.P. Nicolau, J. Pugin, Characteristics of an ideal nebulized antibiotic for the treatment of pneumonia in the intubated patient, Ann. Intens. Care 6 (2016) 35.

[10] D. Honeybourne, Antibiotic penetration into lung tissues, Thorax 49 (1994) 104–106.

[11] M. Cruciani, G. Gatti, L. Lazzarini, G. Furlan, G. Broccali, M. Malena, C. Franchini, E. Concia, Penetration of vancomycin into human lung tissue, J. Antimicrob.

Chemother. 38 (1996) 865–869.
[12] R. Imberti, M. Cusato, P. Villani, L. Carnevale, G.A. Iotti, M. Langer, M. Regazzi, Steady-state pharmacokinetics and BAL concentration of colistin in critically Ill patients after IV colistin methanesulfonate administration, Chest 138 (2010) 1333–1339.
[13] G. Kassab, M.C. Geralde, N.M. Inada, A.E. Achiles, V.G. Guerra, V.S. Bagnato, Nebulization as a tool for photosensitizer delivery to the respiratory tract, J. Biophotonics 12 (2019) e201800189.
[14] J.E. Pennington, Penetration of antibiotics into respiratory secretions, Rev. Infect. Dis. 3 (1981) 67–73.
[15] A. Arnold, S.D. Brouse, W.D. Pitcher, R.G. Hall, Empiric therapy for gram-negative pathogens in nosocomial and health care-associated pneumonia: starting with the end in mind, J. Intens. Care Med. 25 (2010) 259–270.
[16] B.A. Cunha, Antibiotic side effects, Med. Clin. North Am. 85 (2001) 149–185.
[17] A.H. Holmes, L.S.P. Moore, A. Sundsfjord, M. Steinbakk, S. Regmi, A. Karkey, P.J. Guerin, L.J.V. Piddock, Understanding the mechanisms and drivers of antimicrobial resistance, Lancet 387 (2016) 176–187.
[18] M.R. Hamblin, T. Hasan, Photodynamic therapy: a new antimicrobial approach to infectious disease? Photochem. Photobiol. Sci. Offic. J. Euro. Photochem.y Assoc. Euro. Soc. Photobiol. 3 (2004) 436–450.
[19] M. Wainwright, Photodynamic antimicrobial chemotherapy (PACT), J. Antimicrob. Chemother. 42 (1998) 13–28.
[20] M. Wainwright, T. Maisch, S. Nonell, K. Plaetzer, A. Almeida, G.P. Tegos, M.R. Hamblin, Photoantimicrobials—are we afraid of the light? Lancet. Infect. Dis 17 (2017) e49–e55.
[21] Z. Luksiene, A. Zukauskas, Prospects of photosensitization in control of pathogenic and harmful micro-organisms, J. Appl. Microbiol. 107 (2009) 1415–1424.
[22] S. Perni, P. Prokopovich, J. Pratten, I.P. Parkin, M. Wilson, Nanoparticles: their potential use in antibacterial photodynamic therapy, Photochem. Photobiol. Sci. Offic. J. Euro. Photochem. Assoc. Euro. Soc. Photobiol. 10 (2011) 712–720.
[23] M. Raschpichler, M.R. Agel, S.R. Pinnapireddy, L. Duse, E. Baghdan, J. Schäfer, U. Bakowsky, In situ intravenous photodynamic therapy for the systemic eradication of blood stream infections, Photochem. Photobiol. Sci. Offic. J. Euro. Photochem. Assoc. Euro. Soc. Photobiol. 18 (2019) 304–308.
[24] N. Plenagl, B.S. Seitz, S. Reddy Pinnapireddy, J. Jedelská, J. Brüßler, U. Bakowsky, Hypericin loaded liposomes for anti-microbial photodynamic therapy of gram-positive bacteria, Phys. Status Solidi A 14 (2018) 1700837.
[25] L. Duse, E. Baghdan, S.R. Pinnapireddy, K.H. Engelhardt, J. Jedelská, J. Schaefer, P. Quendt, U. Bakowsky, Preparation and characterization of curcumin loaded chitosan nanoparticles for photodynamic therapy, Phys. Status Solidi A 4 (2017) 1700709.
[26] R.R. Allison, G.H. Downie, R. Cuenca, X.-H. Hu, C.J.H. Childs, C.H. Sibata, Photosensitizers in clinical PDT, Photodiagn. Photodyn. Ther. 1 (2004) 27–42.
[27] A. Oniszczuk, K.A. Wojtunik-Kulesza, T. Oniszczuk, K. Kasprzak, The potential of photodynamic therapy (PDT)-Experimental investigations and clinical use, Biomed. Pharmacother. = Biomédecine Pharmacothér. 83 (2016) 912–929.
[28] J. Zhang, L. Wu, H.-K. Chan, W. Watanabe, Formation, characterization, and fate of inhaled drug nanoparticles, Adv. Drug Deliv. Rev. 63 (2011) 441–455.
[29] A. Bohr, C.A. Ruge, M. Beck-Broichsitter, Preparation of Nanoscale Pulmonary Drug Delivery Formulations by Spray Drying, in: D.G. Capco, Y. Chen (Eds.), Nanomaterial: Impacts on Cell Biology and Medicine, Springer, Netherlands, Dordrecht, 2014, pp. 183–206.
[30] N. Anton, A. Jakhmola, T.F. Vandamme, Trojan microparticles for drug delivery, Pharmaceutics 4 (2012) 1–25.
[31] E. Baghdan, L. Duse, J.J. Schüer, S.R. Pinnapireddy, M. Pourasghar, J. Schäfer, M. Schneider, U. Bakowsky, Development of inhalable curcumin loaded Nano-in-Microparticles for bronchoscopic photodynamic therapy, European journal of pharmaceutical sciences official journal of the European Federation for Pharmaceutical Sciences, 2019, pp. 63–71.
[32] R.A. Sharma, W.P. Steward, A.J. Gescher, Pharmacokinetics and pharmacodynamics of curcumin, in: B.B. Aggarwal, Y.-J. Surh, S. Shishodia (Eds.), The Molecular Targets and Therapeutic Uses of Curcumin in Health and Disease, Springer, Boston, MA, 2007, pp. 453–470.
[33] L. Duse, S.R. Pinnapireddy, B. Strehlow, J. Jedelská, U. Bakowsky, Low level LED photodynamic therapy using curcumin loaded tetraether liposomes, Euro. J. Pharm. Biopharm. Offic. J. Arbeitsgemeinschaft fur Pharmazeutische Verfahrenstechnik e.V (2018) 233–241.
[34] M.M. Yallapu, B.K. Gupta, M. Jaggi, S.C. Chauhan, Fabrication of curcumin encapsulated PLGA nanoparticles for improved therapeutic effects in metastatic cancer cells, J. Colloid Interface Sci. 351 (2010) 19–29.
[35] E. Baghdan, M. Raschpichler, W. Lutfi, S. Reddy Pinnapireddy, M. Pourasghar, J. Schäfer, M. Schneider, U. Bakowsky, Nano spray dried antibacterial coatings for dental implants, Eur. J. Pharm. Biopharm. Offic. J. Arbeitsgemeinschaft fur Pharmazeutische Verfahrenstechnik e.V 139 (2019) 59–67.
[36] C.A. Ruge, A. Bohr, M. Beck-Broichsitter, V. Nicolas, N. Tsapis, E. Fattal, Disintegration of nano-embedded microparticles after deposition on mucus: a mechanistic study, Colloids Surf. B, Biointerf. 139 (2016) 219–227.
[37] A. Torge, P. Grützmacher, F. Mücklich, M. Schneider, The influence of mannitol on morphology and disintegration of spray-dried nano-embedded microparticles, Eur. J. Pharm. Sci. Offic. J. Eur. Feder. Pharm. Sci. 104 (2017) 171–179.
[38] M.R. Agel, E. Baghdan, S.R. Pinnapireddy, J. Lehmann, J. Schäfer, U. Bakowsky, Curcumin loaded nanoparticles as efficient photoactive formulations against gram-positive and gram-negative bacteria, Colloids Surf., B 178 (2019) 460–468.
[39] H. Fessi, F. Puisieux, J.P. Devissaguet, N. Ammoury, S. Benita, Nanocapsule formation by interfacial polymer deposition following solvent displacement, Int. J. Pharm. 55 (1989) R1–R4.
[40] J.M. Barichello, M. Morishita, K. Takayama, T. Nagai, Encapsulation of hydrophilic and lipophilic drugs in PLGA nanoparticles by the nanoprecipitation method, Drug Dev. Ind. Pharm. 25 (1999) 471–476.
[41] M. Gaumet, A. Vargas, R. Gurny, F. Delie, Nanoparticles for drug delivery: the need for precision in reporting particle size parameters, Eur. J. Pharm. and Biopharmac. Offic. J. Arbeitsgemeinschaft fur Pharmazeutische Verfahrenstechnik e.V 69 (2008) 1–9.
[42] B.Y. Shekunov, P. Chattopadhyay, H.H.Y. Tong, A.H.L. Chow, Particle size analysis in pharmaceutics: principles, methods and applications, Pharm. Res. 24 (2007) 203–227.
[43] M. Maury, K. Murphy, S. Kumar, L. Shi, G. Lee, Effects of process variables on the powder yield of spray-dried trehalose on a laboratory spray-dryer, Euro. J. Pharm. Biopharmac. Offic. J. Arbeitsgemeinschaft fur Pharmazeutische Verfahrenstechnik e.V 59 (2005) 565–573.
[44] G. Pilcer, K. Amighi, Formulation strategy and use of excipients in pulmonary drug delivery, Int. J. Pharm. 392 (2010) 1–19.
[45] E. Daviskas, S.D. Anderson, J.D. Brannan, H.K. Chan, S. Eberl, G. Bautovich, Inhalation of dry-powder mannitol increases mucociliary clearance, Eur. Respir. J. 10 (1997) 2449–2454.
[46] E. Daviskas, S.D. Anderson, S. Eberl, H.K. Chan, G. Bautovich, Inhalation of dry powder mannitol improves clearance of mucus in patients with bronchiectasis, Am. J. Respir. Crit. Care Med. 159 (1999) 1843–1848.
[47] E. Daviskas, S.D. Anderson, S. Eberl, I.H. Young, Effect of increasing doses of mannitol on mucus clearance in patients with bronchiectasis, Eur. Respir. J. 31 (2008) 765–772.
[48] R. Vehring, Pharmaceutical particle engineering via spray drying, Pharm. Res. 25 (2008) 999–1022.
[49] A. Grenha, B. Seijo, C. Serra, C. Remuñan-López, Chitosan nanoparticle-loaded mannitol microspheres: structure and surface characterization, Biomacromolecules 8 (2007) 2072–2079.
[50] R.C. Boucher, An overview of the pathogenesis of cystic fibrosis lung disease, Adv. Drug Deliv. Rev. 54 (2002) 1359–1371.
[51] S.K. Lai, Y.-Y. Wang, J. Hanes, Mucus-penetrating nanoparticles for drug and gene delivery to mucosal tissues, Adv. Drug Deliv. Rev. 61 (2009) 158–171.
[52] N.N. Sanders, S.C. de Smedt, E. van Rompaey, P. Simoens, F. de Baets, J. Demeester, Cystic fibrosis sputum: a barrier to the transport of nanospheres, Am. J. Respir. Crit. Care Med. 162 (2000) 1905–1911.
[53] L.M. Ensign, C. Schneider, J.S. Suk, R. Cone, J. Hanes, Mucus penetrating nanoparticles: biophysical tool and method of drug and gene delivery, Adv. Mater. 24 (2012) 3887–3894.
[54] M. Dawson, D. Wirtz, J. Hanes, Enhanced viscoelasticity of human cystic fibrotic sputum correlates with increasing microheterogeneity in particle transport, J. Biol. Chem. 278 (2003) 50393–50401.
[55] J. Kirch, A. Schneider, B. Abou, A. Hopf, U.F. Schaefer, M. Schneider, C. Schall, C. Wagner, C.-M. Lehr, Optical tweezers reveal relationship between microstructure and nanoparticle penetration of pulmonary mucus, Proc. Nat. Acad. Sci. United States Am. 109 (2012) 18355–18360.
[56] C.A. Ruge, J. Kirch, C.-M. Lehr, Pulmonary drug delivery: from generating aerosols to overcoming biological barriers—therapeutic possibilities and technological challenges, Lancet Respir. Med. 1 (2013) 402–413.
[57] F.F. Sperandio, Y.-Y. Huang, M.R. Hamblin, Antimicrobial photodynamic therapy to kill gram-negative bacteria, Recent Pat. Anti-Infect. Drug Discov. 8 (2013) 108–120.
[58] G.P. Tegos, M. Anbe, C. Yang, T.N. Demidova, M. Satti, P. Mroz, S. Janjua, F. Gad, M.R. Hamblin, Protease-stable polycationic photosensitizer conjugates between polyethyleneimine and chlorin(e6) for broad-spectrum antimicrobial photoinactivation, Antimicrob. Agents Chemother. 50 (2006) 1402–1410.
[59] T.C. Pagonis, J. Chen, C.R. Fontana, H. Devalapally, K. Ruggiero, X. Song, F. Foschi, J. Dunham, Z. Skobe, H. Yamazaki, R. Kent, A.C.R. Tanner, M.M. Amiji, N.S. Soukos, Nanoparticle-based endodontic antimicrobial photodynamic therapy, J. Endodon. 36 (2010) 322–328.
[60] T.J. Dougherty, C.J. Gomer, B.W. Henderson, G. Jori, D. Kessel, M. Korbelik, J. Moan, Q. Peng, Photodynamic therapy, J. Natl Cancer Inst. 90 (1998).
[61] J. Moan, K. Berg, The photodegradation of porphyrins in cells can be used to estimate the lifetime of singlet oxygen, Photochem. Photobiol. 53 (1991) 549–553.
[62] L. Brancaleon, H. Moseley, Laser and non-laser light sources for photodynamic therapy, Lasers Med. Sci. 17 (2002) 173–186.
[63] T.S. Mang, Lasers and light sources for PDT: past, present and future, Photodiagn. Photodyn. Ther. 1 (2004) 43–48.
[64] I. Yoon, J.Z. Li, Y.K. Shim, Advance in photosensitizers and light delivery for photodynamic therapy, Clin. Endosc. 46 (2013) 7–23.
[65] C.M. Cassidy, M.M. Tunney, N.D. Magee, J.S. Elborn, S. Bell, T.R.R. Singh, R.F. Donnelly, Drug and light delivery strategies for photodynamic antimicrobial chemotherapy (PACT) of pulmonary pathogens: a pilot study, Photodiagn. Photodyn. Ther. 8 (2011) 1–6.
[66] R. Allison, K. Moghissi, G. Downie, K. Dixon, Photodynamic therapy (PDT) for lung cancer, Photodiagn. Photodyn. Ther. 8 (2011) 231–239.